Journal of Fluids and Structures (2002) **16**(5), 649–665
doi:10.1006/jfls.441 available online at http://www.idealibrary.com on IDEAL®

SELF-EXCITED VIBRATION OF A CONTROL VALVE DUE TO FLUID–STRUCTURE INTERACTION

A. Misra[a], K. Behdinan[b] and W.L. Cleghorn[a]

[a] *Department of Mechanical and Industrial Engineering, University of Toronto, Toronto Ontario, Canada M5S 3G8*

[b] *Department of Mechanical Engineering, Ryerson Polytechnic University, Ontario, Canada*

(Received 10 October 2000; and in final form 20 October 2001)

In this paper, the mechanism causing self-excited vibration of a piping system is determined using a dynamic model which couples the hydraulics of a piping system with the structural motion of an air-operated, plug-type automatic control valve. In the dynamic model developed, the structural system consists of a valve spring–mass system, while the fluid system consists of a pump, upstream piping, control valve and downstream piping. The coupling between the structural and the fluid systems at the control valve is obtained by making the fluid flow coefficient at the control valve to be a function of valve plug displacement, and by making the valve plug displacement to be a function of fluid pressure and velocity. The dynamic model presented in this paper, for the first time, considers compressibility of the fluid in both the upstream and downstream piping. The dynamic model presented was benchmarked against *in situ* measurements. The data used for the benchmarking are provided in the paper. A review of the numerical results obtained indicates that the self-excited vibration occurs due to the coincidence of water hammer, acoustic feedback in the downstream piping, high acoustic resistance at the control valve, and negative hydraulic stiffness at the control valve.

1. INTRODUCTION

In a 516 MWe CANDU nuclear reactor, the heat transport system (HTS) is pressurized using feedwater systems. Figure 1 gives a schematic of the feedwater piping system. It consists of a long 2-in (50·8 mm) diameter feed line supplying cold, pressurized heavy water to the HTS header. The system is pressurized using a multi-stage centrifugal pump, and the flow in the feed line is controlled using an air-operated, plug-type automatic control valve. There are two different configurations of the feedwater piping systems. The lengths of the piping system upstream of the control valve are the same in both of the configurations; however, they are different for the piping downstream of the control valve. One of the systems has a downstream piping length of 26 m while the other has a length of 33·3 m. During normal operation, the pressure upstream of the valve is nearly constant (12 MPa), while the pressure downstream of the valve can change significantly depending on the HTS operating pressure (0–9 MPa). Operating experience indicates that the feed lines vibrate under certain operating conditions. Numerous changes to the valve spring and actuators were undertaken; however, the piping vibration persisted. A root cause investigation was initiated to identify the cause of piping vibration. The objective of this paper is to present the analytical studies performed to identify the vibration mechanism and the parameters that control the vibration mechanism.

0889-9746/02/050649 + 17 $35.00/0

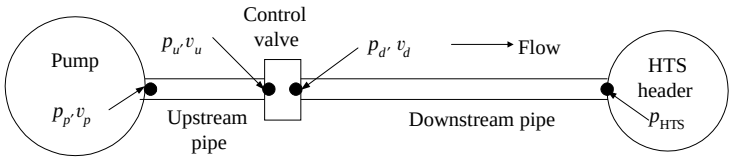

Figure 1. Schematic sketch of the feedwater piping system.

A review of the current and previous measurements indicated that the measured vibration frequencies of the piping systems and the control valve stems were significantly different from the natural frequencies of the pump, valve spring–mass system, and valve–positioner control system. In one of the previous measurements, the feedwater piping systems with downstream piping lengths of 26 and 33·3 m vibrated at frequencies of 14·5 and 10 Hz, respectively. These measured vibration frequencies are close to the acoustic natural frequencies of the downstream piping connecting the valve to the HTS header. It was, therefore, postulated that the piping hydraulics couples with the control valve stem motion and causes the system to vibrate because of self-excited vibration. In this paper, further review and analysis was directed to the dynamic coupling between the piping hydraulics and the valve spring–mass system to determine the self-excited vibration mechanism.

Self-excited vibration due to coupling between structural valve and piping hydraulics has been reported and analysed in literature. According to Naudascher (1977), dynamic modelling of a system with a valve requires modelling of three oscillators: flow oscillator in the valve, body oscillator for the elastically supported valve, and fluid oscillator for the fluid in the piping systems. Each of these oscillators can be modelled using homogenous differential equations and, depending on the coupling term between the three oscillator equations, different types of excitations are obtained. Depending on the excitation mechanism and the feedback mechanism involved, Naudascher has classified the self-excited, flow-induced vibration as fluid-dynamic, fluid-resonant, and fluid-elastic excitation.

Kolkman (1977) has developed a theory to analyse gate valve vibration. His studies indicate that the valve motion introduces hydraulic forces on the valve. When the hydraulic forces generated are proportional to valve displacement, they provide additional stiffness to the valve–spring system; when they are proportional to the valve velocity, they provide additional damping. Kolkman's studies have shown that there are three types of hydraulic forces acting on the valve during valve motion. First, there is a damping effect that occurs when the valve velocity is low. At low valve velocities, the fluid velocity is proportional to the valve opening. This causes the fluid acceleration and therefore the hydraulic load to be proportional to the valve velocity. Second, there is a stiffness effect that occurs when the valve velocity is high. At high valve velocities, because of the fluid inertia the velocity of the flow through the valve does not change significantly with valve displacements. This causes the pressure differential across the valve or the hydraulic force to become directly proportional to the valve displacement in order to maintain the pressure differential versus flow relationship at the valve. Third, there is the viscous damping force which occurs when the valve moves in the fluid volume of the valve body, squeezing the fluid therein through the resistive valve throat. Using this categorization of the forces, Kolkman showed that the onset of unstable vibration can be detected based on negative hydraulic stiffness effect.

Weaver (1979) and Weaver & Ziada (1980) have analysed the self-excited vibration of a check valve in a piping system between two reservoirs. In their analysis, Weaver & Ziada

considered only the fluid inertia effects and neglected the fluid compressibility effects. Their experiments showed that the opening time was much smaller than the closing time, and contrary to intuition, an increase in stiffness decreases the vibration frequency. Weaver & Ziada (1980) demonstrated, using numerical analysis, that the observed behavior occurred because the opening portion of the cycle is controlled by the natural response of the elastic system, while the closing portion of the cycle is controlled by the negative hydraulic stiffness of the hydrodynamic load.

Hayashi & Ohi (1993) and Hayashi *et al.* (1997) have analysed a piping system consisting of poppet valves discharging to atmosphere and connected to a reservoir via a short pipe. They performed valve instability analysis at small valve openings and developed regions of instability for various supply pressures and valve lifts. The instability region expanded with increases in the length of upstream piping and the supply pressure. The paper identified two types of self-excitation: soft and hard. In soft self-excitation, the system is in an unstable region, and a small perturbation causes it to go unstable. For hard self-excitation, the system is in a stable region, and it goes unstable when subjected to large input disturbance.

In the papers reviewed, except for Hayashi & Ohi (1993), none of the papers considered the compressibility of the fluid in the piping. The Hayashi & Ohi (1993) model, however, did not have the model for the piping downstream of the control valve. Further, the self-excited vibration mechanism identified by Hayashi & Ohi is not applicable to the current feedwater piping vibration because the compressibility of the fluid in the upstream piping, as per the more recent paper by Hayashi *et al.* (1997), was not a significant contributor to the vibration mechanism.

In this paper, the dynamic model of the feedwater system that includes the fluid compressibility effects is developed by extending the formulation given by Hayashi & Ohi (1993) to include a pump, downstream piping, valve actuator, fluid on top of the plug, and friction on the valve-stem. The dynamic model is validated against *in situ* measurements and observations, and is used to perform numerical studies to get a better understanding of the dynamic nature of the self-excited vibration mechanism and the parameters controlling the instability. The scope of this paper is limited to determining the onset of valve instability. Appendix A provides the numerical values and units used in the analysis and the definitions of the acronyms and symbols used in the paper.

2. GOVERNING EQUATIONS

A dynamic model was developed for the system shown in Figure 1. In the dynamic model, formulations were developed for the structural valve, the hydraulic system between the pump and HTS header, and the coupling between structural and hydraulic systems at the control valve. The development resulted in a differential equation formulation for the valve–spring mass system and a nonlinear system of equation formulation for the hydraulic system. A Fortran F90 PC program was developed to perform the numerical simulation. The program uses industry standard IMSL routines to perform a Runge–Kutta transient solution for the valve motion and a nonlinear system of equations solver for the hydraulic system.

2.1. Valve Spring–Mass System

The valve, as shown in Figure 2, has an actuator, stem/plug assembly, bellows, spring, and friction plugs. The valve–positioner control system changes the valve opening by

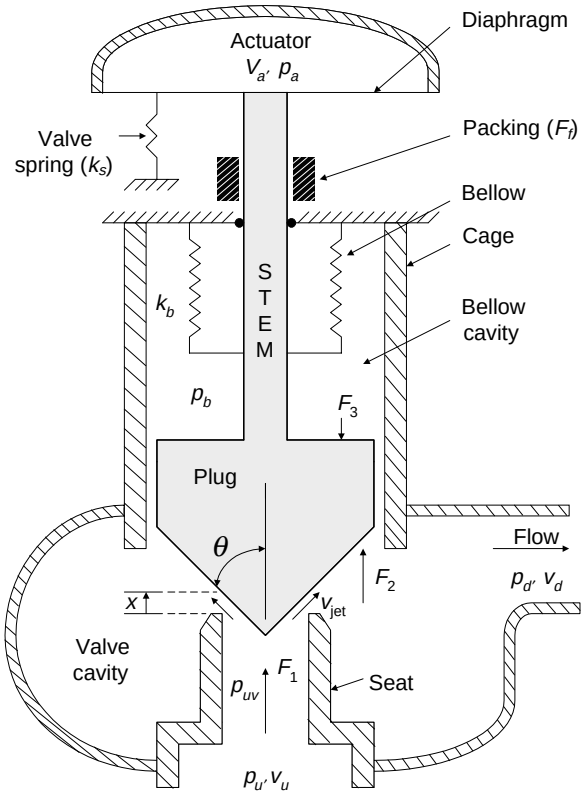

Figure 2. Schematic sketch of the control valve.

controlling the pressure in the actuator. A change in actuator pressure causes the diaphragm to displace and move the valve–stem assembly to the required valve opening.

The dynamic model simulates the valve motion by having the equilibrium valve position required by the valve–positioner system as the user input. A change in equilibrium valve position causes a linear change in the equilibrium actuator air volume and pressure in the dynamic model. Changing actuator pressure causes an unbalanced load on the valve–stem and moves the stem when the unbalanced load is greater than the resistive friction forces and the hydraulic forces of the valve.

Under dynamic conditions, the actuator air pressure and volume are different from the equilibrium values input by the valve–positioner system. This difference exists because the valve displacement relative to the equilibrium valve positions causes a change in actuator air volume and, as per the gas law, also a change in the actuator air pressure. For an isentropic process, the following formulation gives a relationship for actuator pressure as a function of valve displacement and the equilibrium valve displacement:

$$p_a = \left[p_{ac} - (p_{ac} - p_{ao})\frac{x}{x_{\max}}\right]\left(\frac{V_{ac} - A_d x_a}{V_{ac} - A_d x}\right)^{\gamma}, \tag{1}$$

where p_a is the actuator pressure, p_{ac} is the actuator pressure for closed condition, p_{ao} is the actuator pressure for fully open condition, x is the valve displacement, $x_{\max}$ is the total valve travel length, V_{ac} is the actuator volume at closed condition, and x_a is the

equilibrium valve displacement input by the valve–positioner system, and γ is the gas constant.

The change in actuator air pressure causes an unbalanced load on the diaphragm and this causes the valve stem to move. The magnitude of valve displacement depends on: the inertia of the moving parts; stiffness due to valve spring, bellows and accumulator air compressibility; friction due to valve internals and stem packing; and hydraulic forces acting on the valve plug/stem assembly exposed to the fluid system. Newton's second law of motion can be used to obtain equation of motion for the valve as follows:

$$m\ddot{x} + k(x - x_i) + F_f \text{sign}(\dot{x}) + (p_a - p_{ai})A_d + F_e = F_h, \tag{2}$$

where x_i is the initial steady-state valve displacement, m the total effective mass of the valve/stem assembly, k the stiffness due to spring and bellows, F_f the plug friction force, F_e the initial equilibrium hydraulic force, A_d the area of the diaphragm, p_a the actuator air pressure, p_{ai} the initial pressure in the actuator, and F_h the hydraulic force acting on the valve plug.

2.2. Hydraulic Interaction Force on Valve

Figure 2 shows the valve–plug surfaces where the hydraulic system applies the wall friction and thrust forces. The wall friction force occurs on the wall between the plug and the cage as the fluid flows in and out of the bellows cavity during valve motion. The hydraulic force has three components, F_1, F_2, and F_3, acting on the three surfaces of the valve–plug. Force component F_1 is due to the pressure upstream of the control valve and acts on the bottom surface of the plug. Force component F_2 is due to the pressure downstream of the valve and acts on the bottom surface of the plug excluding the seat area. Force component F_3 is due to the pressure in the bellows cavity region and acts on the top surface of the plug. Hayashi *et al.* (1997) provide a formulation for estimating force F_1. This formulation is extended to include the effect of F_2, F_3 and friction force to calculate the total hydraulic force, F_h, on the valve–plug as follows:

$$\begin{aligned} F_h = {} & [A_{\text{seat}} p_u - \dot{m}_v v_{\text{jet}} \cos\theta] \\ & + [(A_{\text{plug}} - A_{\text{seat}})p_d - (A_{\text{plug}} - A_{\text{bellow}})p_b] + [0{\cdot}5(A_{\text{cage}} - A_{\text{plug}})(p_d - p_b)], \end{aligned} \tag{3}$$

where p_u, p_d and p_b are the pressures in the piping system just upstream of the control valve, downstream of the control valve and in the bellows cavity, respectively; $\dot{m}_v$is the mass flow rate through the control valve, v_{jet} the velocity of the jet exiting the valve; θ the half valve-plug angle, and A_{seat}, A_{plug}, A_{bellow} and A_{cage} are the areas of valve seat, plug, bellows and cage, respectively.

The mass flow rate through the valve is determined using the following formula for the fluid parameters in the SI units:

$$\dot{m}_v = 2{\cdot}402 \times 10^{-5} \rho c_v \sqrt{\frac{p_u - p_d}{\rho}}, \tag{4}$$

where ρ is the density of fluid, and c_v is the flow coefficient. Figure 3 gives the manufacturer's suggested static flow coefficient as a function of valve position. This curve is normally obtained experimentally under static flow conditions. In this paper, it is assumed that the flow coefficient curve for static flows can be used for dynamic analysis.

The fluid velocity of the jet exiting the control valve is a function of the pressure differential across the control valve. Using Bernoulli's equation, the jet velocity can be

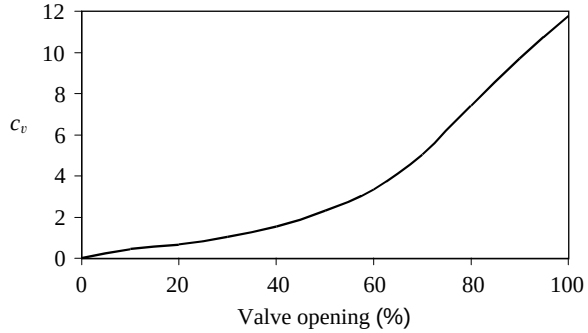

Figure 3. Static flow coefficient C_v versus percent valve opening.

obtained as follows:

$$v_{\text{jet}} = \sqrt{\frac{2(p_{uv} - p_d)}{\rho}},$$

$$p_{uv} = p_u + 0.5\rho v_u^2 \left[1 - \frac{A_{\text{pipe}}^2}{A_{\text{seat}}^2}(1 + k_{\text{inlet}})\right], \tag{5}$$

where p_{uv} is the pressure upstream of the valve under the plug, v_u the fluid velocity in the pipe upstream of the valve, k_{inlet} the minor head-loss coefficient in the valve seat upstream of the plug, and A_{pipe} the area of the pipe.

2.3. Hydraulic System

The hydraulic system is made up of four elements: pump, upstream piping, control valve, and downstream piping. In this section, the state of the hydraulic system will be defined using nine variables that are related using nine equations.

The pump used in the system is a high pressure, low flow pump. Figure 4 gives the pump flow curve relating the pump head and the mass flow rates. This relationship can be expressed mathematically as follows:

$$p_p = \text{f}(\dot{m}_p) = \text{f}(\rho A_{\text{pipe}} v_p), \tag{6}$$

where p_p is the pressure head generated by the pump, v_p the fluid velocity in the pipe at the pump exit, and $\dot{m}_p$ the mass flow rate through the pump.

The pressure and velocities at the pump can be related to the pressure and velocities at the downstream end of the upstream piping using the wave solution to the Navier–Stokes equations of motion of nearly incompressible fluids:

$$p_u(t) + z_0 v_u(t) = p_p(t - T_u) + z_0 v_p(t - T_u), \tag{7}$$

$$p_p(t) - z_0 v_p(t) = p_u(t - T_u) - z_0 v_u(t - T_u), \tag{8}$$

where z_0 is the characteristic impedance of the piping system (ρc), and T_u is the acoustic wave travel time from the control valve to the pump. In equations (7) and (8), the pipe-wall shear effects are ignored because the length of the upstream piping is small, and the acoustic waves are assumed to be one-dimensional planar waves because the pipe dimensions are small compared to the acoustic wavelength.

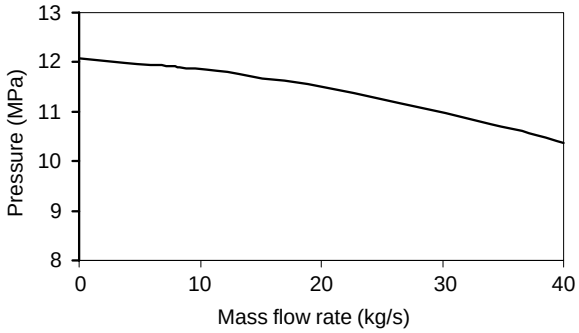

Figure 4. Pump flow curve.

The downstream piping starts from the control valve and ends in the HTS header. The HTS header is modelled as a constant pressure reservoir because of its large diameter and volume when compared to the downstream piping. The pressure and velocities downstream of the control valve at a given instant can be expressed as a function of the values at a previous instant using the wave solution as follows:

$$p_d(t) - z_0 v_d(t) = 2\left(p_{\mathrm{HTS}} + \frac{k_{\mathrm{outlet}}\rho v_d^2(t)}{2}\right) - p_d(t - 2T_d) - z_0 v_d(t - 2T_d), \tag{9}$$

where p_{HTS} is the HTS header pressure, v_d is the fluid velocity in the pipe downstream of the valve, k_{outlet} is the head loss coefficient in the downstream piping, and T_d is the acoustic wave travel time from the control valve to the HTS header.

The valve discharge equation, which relates pressures upstream and downstream of the control valve, can be obtained by dividing equation (4) by the fluid density as follows:

$$q_v = A_{\mathrm{pipe}} v_v = 2{\cdot}402 \times 10^{-5} c_v \sqrt{\frac{p_u - p_d}{\rho}}, \tag{10}$$

where q_v and v_v are the volume flow rate and velocity through the valve for a stationary valve. In this formulation, the acceleration of the fluid in the valve bowl is omitted as the volume of the fluid in the bowl is small compared to the fluid in the piping.

The fluid velocities at the valve and the stem motion are related. The valve plug motion displaces fluid in the bowl cavity. Some of the fluid flows into the upstream and downstream piping, while the rest flows into the bellows cavity. Given the small size of the bellows cavity and valve bowl, the compressibility of the fluid is neglected and is assumed to be incompressible. Next, using the continuity equation, the stem motion and the fluid velocities at the control valve can be related as follows:

$$v_u = v_v + \frac{A_{\mathrm{seat}}}{A_{\mathrm{pipe}}}\dot{x}, \tag{11}$$

$$v_d = v_v - \frac{(A_{\mathrm{plug}} - A_{\mathrm{seat}})}{A_{\mathrm{pipe}}}\dot{x} - (A_{\mathrm{cage}} - A_{\mathrm{plug}})v_b, \tag{12}$$

where v_b is the fluid velocity in the annular gap between the cage and the plug, and can be expressed as follows:

$$v_b = -\frac{A_{\mathrm{cage}} - A_{\mathrm{bellow}}}{A_{\mathrm{cage}} - A_{\mathrm{plug}}}\dot{x}. \tag{13}$$

The fluid flow in the annular gap between the cage and the plug is assumed to be laminar. The friction pressure drop can be calculated using the following equation:

$$p_d - p_b = \frac{8\pi\mu L v_b}{(A_{\text{plug}} + A_{\text{cage}}) - 2(A_{\text{cage}} - A_{\text{plug}})/\ln(A_{\text{cage}}/A_{\text{plug}})}, \tag{14}$$

where μ is the dynamic viscosity of the fluid, and L is the length of the plug with annular fluid flow.

This completes the development of the mathematical formulation for the hydraulic system. The development resulted in a system of nine equations, equations (6)–(14), to solve nine unknown pressure and velocity variables, p_p, v_p, p_u, v_u, v_v, p_d, v_d, p_b and v_b. The system of equations can be solved to obtain the hydraulic state at various instances.

3. IN SITU MEASUREMENTS

In-service inspection of the feedwater system revealed support failures in the feed line piping. Assessment of these failures indicated that the feed line piping had been subjected to high vibration. High level of vibration was not observed during normal operations, so *in situ* measurements were performed to identify the operating conditions corresponding to high piping vibration.

The *in situ* measurements consisted of monitoring stem movement and piping accelerations at multiple locations for various valve positions and downstream HTS header pressure conditions. These measurements indicated that the system is stable for most operating conditions. However, when the downstream pressure was at 4 MPa, and the valve was closing from 70 to 62% valve opening, the system went into self-excited vibration.

Figure 5(a–c) gives plots of the stem movement at three different times during the vibration event. Figure 5(a) plots the initiation of the valve instability. Each reversal in vibration direction shows the characteristic backlash effect due to the stem packing friction force. The magnitude of valve vibration increases with each cycle, and valve vibration has a frequency of 12 Hz. Figure 5(b) shows that at high vibration levels, the stem has steady state, limit-cycle type vibration. During steady state vibration, the vibration frequency was 13 Hz and the stem motion was between 57 to 75% valve openings. Figure 5(c) plots the termination of valve vibration as the valve opening is decreased to 42% valve opening. In the 42–50% valve opening range, the valve was vibrating at around 14 Hz.

4. ANALYSIS

Numerical simulations were performed to validate the dynamic model against these *in situ* measurements, to identify the self-excited vibration mechanism, and to determine the parameters controlling the onset of instability. In the analysis, a time step of 0·002 s was used. Sensitivity studies of the iteration time step were performed to ensure convergence of the solution.

4.1. Model Validation

The validation exercise consisted of reproducing numerically the regions of valve opening and HTS pressure conditions where the system vibration occurred. Two sets of runs were performed. In one, the initial valve opening was changed, and in the other, the downstream header pressure was changed.

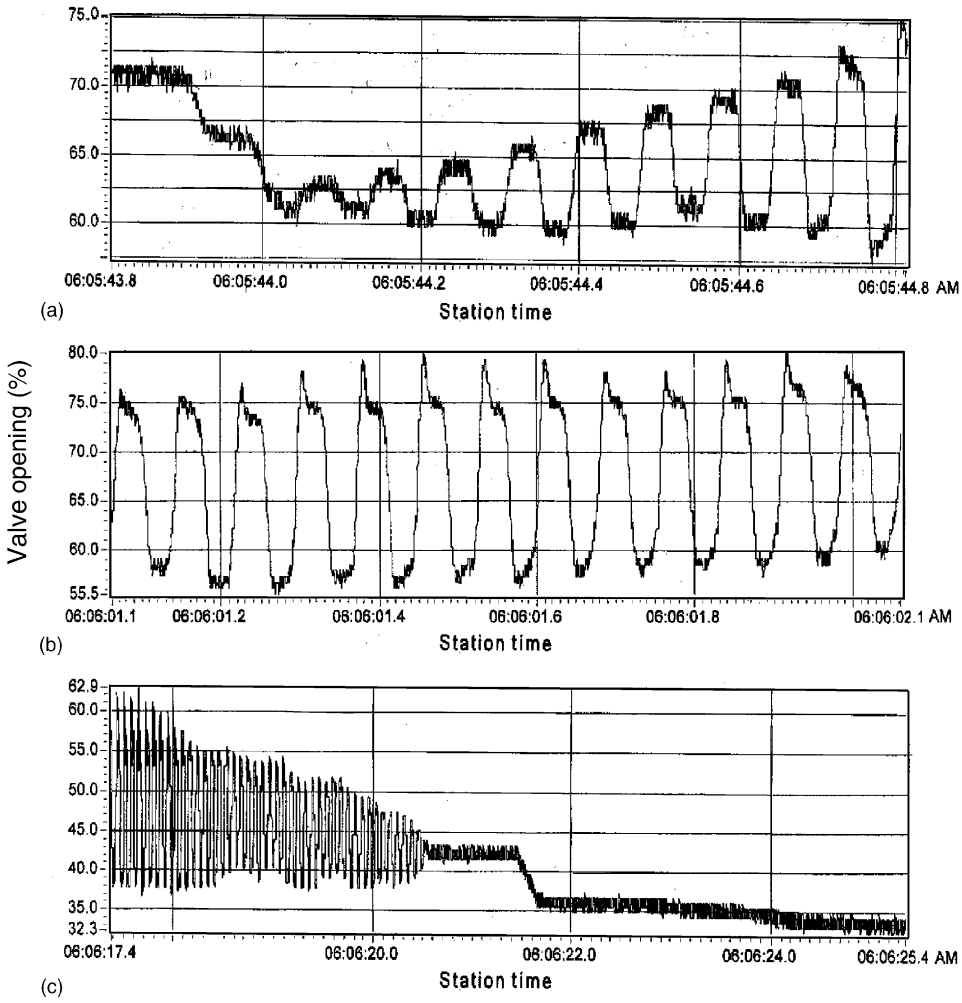

Figure 5. Time–histories of *in situ* measured valve stem vibration (HTS header pressure = 4 MPa): (a) initiation stage of valve vibration (12 Hz); (b) steady-state valve vibration (13 Hz); (c) ending stage of vibration (14 Hz).

Figure 6 gives the time–history plots of stem displacements for multiple valve-closing transients at different initial valve opening positions. Each transient consists of 8% valve closing in 0·05 s with the HTS header pressure kept constant at 4 MPa. The initial equilibrium valve opening positions was changed from 90 to 50% valve opening. Figure 6 shows that the system is stable for initial valve openings greater than 80% and smaller than 60%, but unstable for transients at initial valve opening around 60–80%. This result is consistent with the *in situ* measurements.

Figure 7 gives the time–history plots of the stem displacements for multiple valve-closing transients with different HTS header pressure. Each transient has 70% initial valve opening, and is subjected to 8% valve closing in 0·05 s. The HTS pressure ranged from 3 to 6 MPa. Figure 7 shows that the system is unstable when the HTS header pressure is below 5 MPa and magnitude of self-excitation increases as the HTS pressure is decreased below this value. This is consistent with the *in situ* measurements of acceptable valve response under normal operation when the HTS pressure is around 9 MPa. When the HTS

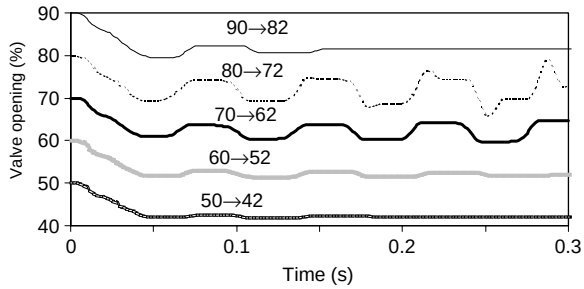

Figure 6. Time–histories of valve stem vibrations due to numerical simulation of valve-closing transients at different initial valve openings.

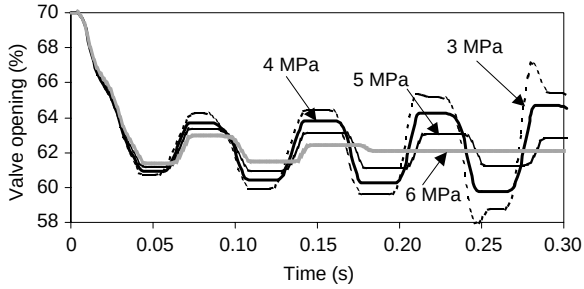

Figure 7. Time–histories of valve stem vibrations due to numerical simulation of valve-closing transients at different HTS header pressures.

pressure is decreased below 5 MPa, the system goes unstable and experiences self-excited vibration.

The 8% valve-closing transient at initial valve opening of 70% and 4 MPa HTS header pressure closely matches the *in situ* measurements and is considered the reference case for further analysis. Figure 8(a) compares the stem displacement for the reference case against the *in situ* measured response shown in Figure 5(a). Comparison of the two responses shows that the dynamic model is able to reproduce the instability, but gives a vibration frequency of 14 Hz which is slightly higher than the measured frequency of 12 Hz. This discrepancy is acceptable because of the differences between the actual system values and the values used in the numerical simulation. For example, it is possible to have an error in the actuator air volume used in the analysis. As shown in Figure 8(b), an increase of only 10% in equilibrium actuator air volume at 62% valve opening results in excellent agreement between the experimental and the numerical simulations for the vibration response.

In addition to the study described in this paper, an attempt was also made to reproduce the measured *in situ* steady-state vibration. During steady-state vibration, voiding occurs downstream of the control valve. The voiding was modelled as a column separation and rejoining process. This attempt was unsuccessful in reproducing the vibration frequency and response profiles. It is possible that, as suggested by Szumowski & Meier (1982), the actual voiding phenomenon is very complex consisting of choked flow through the valve, multiple occurrence of voiding in a single vibration cycle, and void detachment and transport in to the piping system. A more sophisticated model of voiding would be required to properly simulate the steady-state valve response. This sophisticated void modelling was considered beyond the scope of this paper because the objective of the

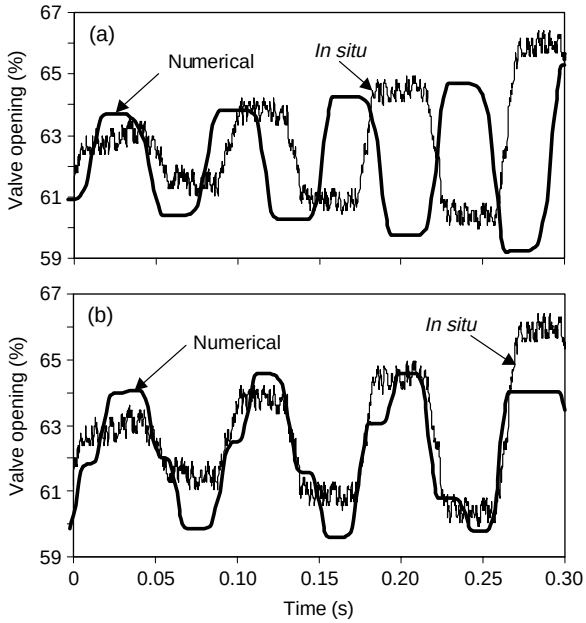

Figure 8. Comparison of numerical simulation and *in situ* measurements: (a) unadjusted actuator air volume; (b) actuator air volume increased by 10%.

analysis was to understand the conditions causing the instability and not to study the response during the unstable self-excited vibration. Under normal operations, when there is no self-excited vibration, there occurring no voiding in the feed line piping.

4.2. Self-Excited Vibration Mechanism

A study of the system response indicates that the self-excited vibration is due to co-incidence of negative hydraulic stiffness, water hammer, high acoustic resistance at the valve, and acoustic feedback. The negative hydraulic stiffness occurs because the hydraulic system introduces an incremental external hydraulic force on the plug in the same direction as the valve motion. The magnitude of the hydraulic force depends on the water hammer pressure generated at the valve during a valve-closing transient and the hydraulic resistance at the valve. The valve keeps vibrating because of the feedback of acoustic pressures in the downstream piping between the control valve and the HTS header. When the incremental hydraulic force is greater than the valve resistance, valve instability can occur.

Figures 9 and 10 are used to illustrate the proposed vibration mechanism. Figure 9, for the reference transient, gives the time–history plots of the system response: valve displacement, pressure upstream of valve, pressure downstream of valve and fluid velocity through the valve. Figure 10 gives time–history plots of water hammer pressures—change in downstream pressure as compared to the initial pressure—for the transients shown in Figure 6.

Figure 9 indicates that during the initial valve-closing phase, the velocity of the flow through the valve decreases and causes pressure change at the valve due to water hammer effects. Upstream of the valve, the pressure increases, while downstream of the valve the pressure decreases. These pressure fluctuations travel in the piping system away from the

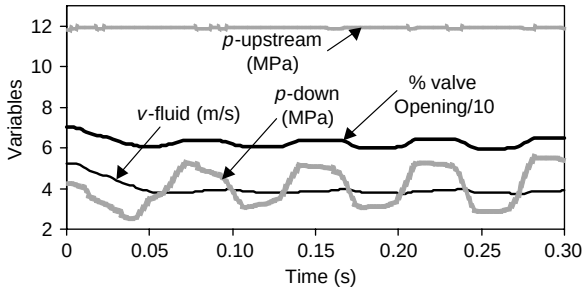

Figure 9. Time–history response of system parameters for reference transient (numerical simulation, 70 to 62% valve closing in 0·05 s, HTS header pressure $p = 4$ MPa).

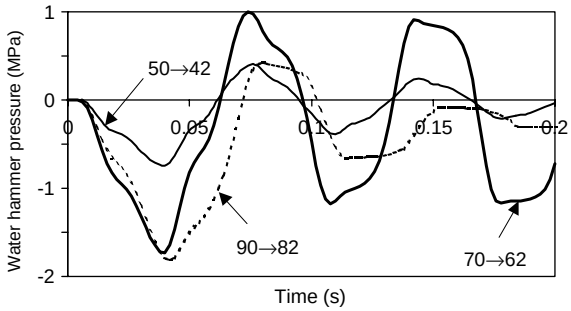

Figure 10. Time history of water hammer pressures downstream of the valve for three valve-closing transients (numerical simulation, HTS Header $p = 4$ MPa).

control valve at acoustic wave speed. Since the pump is close to the valve (< 1 m), the pressure pulsation upstream of the valve is quickly reflected back to the control valve, and this makes it difficult to maintain the upstream pressure fluctuations for long, and no significant water hammer pressures are created. The pressure fluctuations downstream of the valve, however, are easier to maintain for a longer duration because the pressure fluctuations have to travel 23 m to reach the HTS header and then reflect back the same distance to the control valve.

Figure 10 gives time–history plots of water hammer pressures—change in downstream pressure as compared to the initial pressure—for the transients plotted in Figure 6. The water hammer pressure initially decreases monotonically with time. The decrease in pressure is proportional to the total velocity change at the valve. The water hammer pressure keeps decreasing until there are no reflected pressure waves from the HTS header. At the moment when the initial waves generated at the control valve and reflected back from the HTS header start arriving back at the control valve, the pressure stops decreasing and starts rising, and the peak negative pressure is obtained. As expected, the magnitude of initial negative water hammer pressure increases for transients that have higher magnitude of fluid velocity change during the transient. The transients with 70 and 90% initial valve opening have initial peak water hammer pressures that are about three times greater than those obtained for the transient with 50% initial valve opening. This reduction in the water hammer pressure for transients at small opening explains why the valve instability is not obtained when transients occur below 50% valve openings for all operating conditions. Similarly, low water hammer pressures are expected for conditions when the HTS pressure is increased. The increase in HTS pressure causes the pressure

differential across the valve to decrease, and thereby reduces the fluid velocity changes across the valve during transient conditions. This explains why the vibrations do not occur at normal operating conditions when the HTS pressure is around 9 MPa.

Figures 9 and 10 show that when the reflected wave starts arriving at the valve, the pressure downstream of the valve stops decreasing and starts increasing, the valve stops moving downward, and the fluid velocity through the valve stops decreasing. The positive peak water hammer pressure, just like for negative peak pressures, are reached when the increasing water hammer pressures generated at the valve are reflected back to the valve from the HTS header. The time duration between positive and negative peaks depends on the time it takes for an acoustic wave to travel to the HTS system and back to the control valve.

The peak positive water hammer pressure, however, is not proportional to the peak negative pressure. The peak positive water hammer pressure for the transient at 90% valve opening is smaller than that obtained for the transient at 70% valve opening, even though the latter transient had a slightly larger initial negative water hammer pressure. The smaller peak positive water hammer pressure for larger valve opening occurs because the hydraulic resistances at the control valve to pressure fluctuations decreases at higher valve openings. Regetz (1960) has demonstrated this behaviour in an orifice-terminated long tube. In his experiments, as the mean flow through the orifice was increased, the hydraulic resistance through the orifice increased, and after a certain flow rate the orifice-end of the tube changed from an acoustically open to an acoustically closed condition. In the control valve, the flow resistance at the valve for a given flow rate can change due to the changes in the valve opening. As the hydraulic resistance decreases with larger valve openings, beyond a certain valve opening, the valve appears as an acoustically open condition and attenuates the build-up of positive pressure at the valve. A study of the hydraulic resistance of the control valve used in the feedwater system had shown that the transition from an acoustically closed to an open condition occurs at around 80% valve opening. This loss of hydraulic resistance at large valve openings explains the cause of stable valve response for valve openings greater than 80% valve opening.

The valve starts vibrating due to acoustic feedback of acoustic pressure waves reflecting back and forth between the control valve and the HTS header. A review of Figure 9 shows that during vibration the upstream pressure and fluid velocity is nearly constant. The piping downstream of the valve has the characteristic quarter-wavelength acoustic response with pressure antinode at the valve location, and pressure node at the HTS header. The coupled vibration frequency of 14 Hz is slightly lower than the purely acoustic natural frequency of 15·1 Hz. As explained before, this difference is due to coupling effect of valve spring–mass system with the acoustics of the downstream feed line piping. The flexible valve at the upstream end of the downstream piping adds flexibility to the acoustic column in the downstream piping. The effect of this flexibility is to lower the coupled system vibration frequency. Since the mean stiffness of the actuator air depends on the actuator air mass, mean volume and mean pressure, and these variables are changing during the transient, we expect the vibration frequency to change also, as observed in the *in situ* measurements. The maximum frequency, however, will be limited, as observed by the purely acoustic natural frequency of the downstream piping of 15·1 Hz.

Once the valve instability has been initiated, the valve oscillations keep increasing with each cycle until it reaches a limit cycle of pressure as determined by the pressure upstream of the pump ($\sim$12 MPa) and the saturation pressure of the liquid (8 kPa). As the valve natural frequency is significantly higher than the self-excited vibration, the valve displacement can be estimated using the total stiffness of the valve. Combining equations

(1)–(3), dropping the valve inertia term, and considering only F_2 component of the hydraulic load gives the following equation for the steady-state stem vibration:

$$p_u(A_{\text{bellow}} - A_{\text{seat}}) - 2F_f = \left[p_{ac} - (p_{ac} - p_{ao})\frac{x_a}{x_{\max}}\right]\left\{1 - \left[\frac{V_{ac} - A_d(x_a + 0{\cdot}5\Delta x)}{V_{ac} - A_d(x_a - 0{\cdot}5\Delta x)}\right]^{\gamma}\right\}A_d + k\Delta x, \tag{15}$$

where Δx is the peak to peak total stem displacement. Each term in equation (15) represents the range of forces in a given cycle on the valve–stem assembly during a steady-state vibration. The two terms on the left-hand side of equation (15) represent the external force on the valve–stem assembly due to the hydraulic pressure and plug friction. The two terms on the right hand side of equation (15) are the forces on the valve due to the stiffness of the actuator air pressure and the valve spring. Solving equation (15), using the values given in Appendix A for mean valve opening of 62%, results in the stem motion of 22% of valve travel, which is close to the *in situ* measured values of 18% during steady-state valve vibration.

4.3. Parametric Studies

The mechanism described above has identified four components for initiation of self-excited vibration: water hammer, hydraulic resistance at the control valve, acoustic feedback, and the negative hydraulic stiffness. Vibration alleviation methods that provide barriers against any of these components were analysed. In proposing the three methods, options that required modifications of the piping system were not considered, as they were impractical for an in-service system. Changes to operating procedures and valve internals were the only options considered for the parametric study.

The first option analysed was the modification to the positioner control system by slowing down the valve-closing rates. A slow down in the valve-closing rate reduces the magnitude of the first negative water hammer peak in the system and thereby provides as a barrier against initiation of valve vibration. Figure 11 shows the stabilizing effect of increasing the valve closing time from 0·05 s to 0·1 s for the reference transient.

The second option studied was increasing the valve capacity to resist the negative hydraulic stiffness effects during hydraulic transients. The valve resistance can be increased by increasing the valve stiffness or valve damping. As the valve spring was already too large for the size of the valve actuator, increasing it further was not considered. Installing viscous damping snubbers on the stem or using larger values of stem packing friction were viable options. In this paper, only the latter option was analysed by doing a numerical

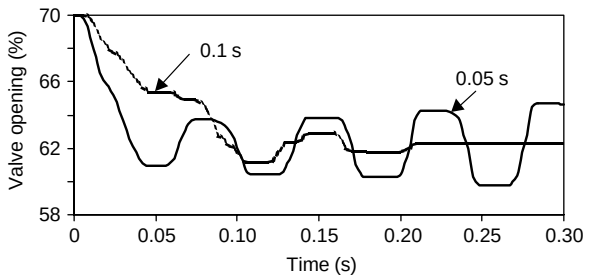

Figure 11. Effect of different valve closing period on valve vibration (numerical simulation, 70 → 62% valve closing transient, HTS Header $p = 4$ MPa).

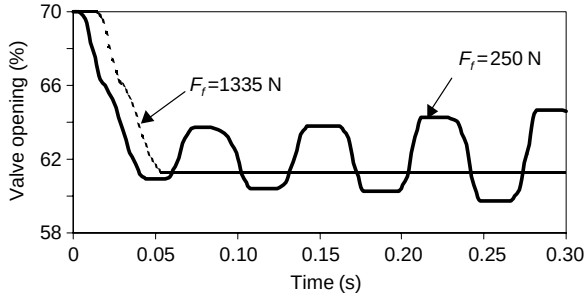

Figure 12. Effect of valve stem plug friction on valve vibration (numerical simulation: 70 → 62% valve closing in 0·05 s, HTS header $p = 4$ MPa).

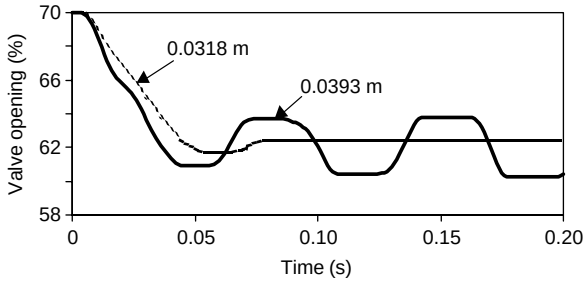

Figure 13. Effect of decreasing bellows diameter on valve stem vibration (numerical simulation, 70 → 62% valve closing in 0·05 s, HTS header $p = 4$ MPa).

simulation in which the stem packing force was increased from 250 to 1335 N. Figure 12 shows that this increase in stem packing friction force can stabilize the stem motion and prevent the self-excited vibration mechanism.

The third option studied was to decrease the negative hydraulic stiffness effects. This can be accomplished by decreasing the interaction area on which the hydraulic resistance acts, for example by changing the bellows diameter. Figure 13 shows the effect of changing the bellows diameter. Decreasing the bellows diameter from 3·94 to 3·18 cm resulted in a stable system response.

The suitability of options studied in this paper needs further assessment of their practicality and impact on other processes. For example, the stem packing friction values may be hard to maintain after a few cycles of normal valve operation, or slowing of valve due to modifications in the positioner–control system or increased valve damping may not be acceptable to the HTS pressure control.

5. CONCLUSION

A fluid–structure dynamic model of the control valve circuit was developed. The model was able to reproduce the *in situ* measurements and the range of operating conditions where the self-excited vibration occurred. A mechanism to explain the self-excited vibration mechanism was developed and the factors initiating the self-excited vibration mechanism were identified. Based on the factors identified, studies were performed to suggest possible solutions to the problem.

ACKNOWLEDGEMENTS

The authors thank Kinetrics Inc. for performing and providing the *in situ* measurements, and Ontario Power Generation Nuclear for providing an opportunity to work on this project, giving approval for using the *in situ* vibration measurements and providing comments and suggestions for this research.

REFERENCES

HAYASHI, S. & OHI, K. 1993 Global stability of a poppet valve circuit. *Journal of Fluid Control* **21,** 48–63.

HAYASHI, S., HYASE, T. & KURAHASHI, T. 1997 Chaos in a hydraulic control valve. *Journal of Fluids and Structures* **11,** 693–716.

KOLKMAN, P. A. 1977 Self-exciting gate vibration. In *Proceedings 17th Congress of International Association for Hydraulic Research*, Vol. 4, pp. 372–381.

NAUDASCHER, E. 1977 Flow-induced vibrations–a unified approach. In *Proceedings 17th Congress of the International Association for Hydraulic Research*, Vol. **6**, pp. 361–369.

REGETZ, J. D., Jr. 1960 An experimental determination of the dynamic response of a long hydraulic line. NASA Technical Note D-576.

SZUMOWSKI, A. P. & MEIER, G. E. A. 1982 Self-induced pulsating liquid flow in a hydraulic system. In *International Conference on Flow Induced Vibrations in Fluid Engineering*, Reading, England, pp. 277–300.

WEAVER, D. S. 1979 Flow induced vibration in valves operating at small openings. In *Practical Experiences with Flow-Induced Vibrations* (eds E. Naudascher & D. Rockwell), pp. 305-319. Berlin: Springer-Verlag.

WEAVER, D. S. & ZIADA, S. 1980 A theoretical model for self-excited vibration in hydraulic gates, valves and seals. *ASME Journal of Pressure Vessel Technology* **102**, 129–135.

APPENDIX A

Acronyms, Nomenclature, Units and Numerical Values used in the Analysis

Symbol	Value	Units	Quantity
A_{bellow}	$1{\cdot}22 \times 10^{-3}$	m^2	area of bellows
A_{cage}	$1{\cdot}44 \times 10^{-3}$	m^2	area of the cage around the valve plug
A_d	$1{\cdot}42 \times 10^{-1}$	m^2	area of the actuator diaphragm
A_{pipe}	$1{\cdot}91 \times 10^{-3}$	m^2	area of feed line piping
A_{plug}	$1{\cdot}43 \times 10^{-3}$	m^2	area of the valve plug
A_{seat}	$2{\cdot}85 \times 10^{-4}$	m^2	area of fluid jet inside the valve seat
CANDU			Canadian Deuterium Uranium
c	1410	m/s	acoustic wave speed in the fluid
c_v			flow coefficient (Figure 3)
F_1, F_2, F_3		N	hydraulic force components acting on the valve.
F_e		N	equilibrium hydraulic force
F_f	250	N	friction force due to stem packing
F_h		N	hydraulic force on the valve plug
HTS			heat transport system
k	$9{\cdot}25 \times 5$	N/m	total stiffness due to valve spring and bellows
k_{inlet}	1·0		head loss coefficient at valve inlet
k_{outlet}	17·0		head loss coefficient in piping downstream of valve
L	0·0254	m	vertical, nontapered length of valve plug

L_d	23·28	m	length of pipe between valve and hts header
L_u	0·9404	m	length of pipe between pump and valve
m	18·2	kg	moving mass of the valve
$\dot{m}_p$		kg/s	fluid mass flow rate through the pump
$\dot{m}_v$		kg/s	fluid mass flow rate through the valve
p_a		Pa	air pressure in the actuator
p_{ac}	$3{\cdot}46 \times 5$	Pa	actuator air pressure at 0% valve opening
p_{ai}		Pa	initial steady-state actuator air pressure
p_{ao}	$2{\cdot}15 \times 5$	Pa	actuator air pressure at 100% valve opening
p_b		Pa	pressure in the bellows cavity
p_d		Pa	pressure downstream of valve
p_{HTS}		Pa	HTS header pressure
p_p		Pa	pump discharge pressure
p_u		Pa	pressure upstream of valve
p_{uv}		Pa	pressure upstream of valve under the seat
q_v		m^3/s	volume flow velocity through the valve
t		s	time of transient
T_d	$1{\cdot}65 \times 10^{-2}$	s	wave travel time from valve to HTS header, L_d/c
T_u	$6{\cdot}67 \times 10^{-4}$	s	Wave travel time from valve to pump, L_u/c
V_{ac}	$5{\cdot}93 \times 10^{-3}$	m^3	volume of actuator air in the closed position
v_b		m/s	fluid velocity in the annular gap region between valve plug and cage entering the bellows cavity
v_d		m/s	fluid velocity downstream of valve
v_{jet}		m/s	fluid velocity of the jet exiting the valve
v_p		m/s	pump discharge velocity
v_u		m/s	fluid velocity upstream of valve
v_v		m/s	fluid velocity through the valve averaged in terms of pipe areas attached to the valve
$x, \dot{x}, \ddot{x}$		m, m/s $\mathrm{m/s}^2$	valve displacement, velocity and acceleration
Δx		m	Peak-to-peak steady-state valve displacement
x_a		m	valve position input by positioner–control system
x_I		m	initial steady-state valve displacement
$x_{\max}$	$1{\cdot}91 \times 10^{-2}$	m	total valve travel distance
Z_0	$1{\cdot}56 \times 6$	$\mathrm{kg/m}^2$ s	characteristic impedance of the fluid, ρc
γ	1·4		adiabatic gas constant
θ	20	deg	half angle of the valve plug bottom surface
μ	$4{\cdot}6 \times 10^{-4}$	kg/m s	dynamic viscosity of fluid
ρ	1105	$\mathrm{kg/m}^3$	fluid density